

**Atomistic mechanism leading to complex antiferroelectric and incommensurate perovskites**Kinnary Patel,<sup>1</sup> Sergey Prosdandev,<sup>1,2</sup> Yurong Yang,<sup>1</sup> Bin Xu,<sup>1</sup> Jorge Íñiguez,<sup>3</sup> and L. Bellaiche<sup>1</sup><sup>1</sup>Physics Department and Institute for Nanoscience and Engineering, University of Arkansas, Fayetteville, Arkansas 72701, USA<sup>2</sup>Institute of Physics and Physics Department of Southern Federal University, Rostov-na-Donu 344090, Russia<sup>3</sup>Materials Research and Technology Department, Luxembourg Institute of Science and Technology, 5 avenue des Hauts-Fourneaux, L-4362 Esch/Alzette, Luxembourg

(Received 22 March 2016; revised manuscript received 8 June 2016; published 12 August 2016)

An atomic interaction is identified in all perovskite compounds, such as  $ABO_3$  oxides, that can potentially result in unconventional structures. The term is harmonic in nature and couples the motions of the  $A$  cations with the rotations of the oxygen octahedra in the perovskite lattice. When strong enough, this coupling leads to *hybrid* normal modes that present both (anti)polar and rotational characters, which are keys to understand a variety of exotic phases. For example, we show that not only does this new coupling explain the long-period soft phonons characterizing prototype antiferroelectric  $PbZrO_3$ , but it also provides us with an unified description of the complex antipolar structures of a variety of perovskites, including the possible occurrence of incommensurate phases. This coupling is further demonstrated to result, in the continuum limit, in an energy invariant adopting an analytical form that has been previously overlooked, to the best of our knowledge.

DOI: [10.1103/PhysRevB.94.054107](https://doi.org/10.1103/PhysRevB.94.054107)**I. INTRODUCTION**

Antiferroelectrics (AFE) form a class of important materials that are currently receiving a lot of attention, mainly because they are promising candidates for obtaining high-density energy storage [1–5]. They are also fundamentally challenging and interesting, as, e.g., demonstrated by recent activities aimed at understanding the unusual ground state of the prototype compound  $PbZrO_3$  (PZO) [6–12].

PZO's ground state displays the  $Pbam$  symmetry and is mostly characterized by two strongly unstable soft phonon modes [6–9,12]. The first of these modes is labeled  $R_4^+$  according to its symmetry, and is rather simple: it features the typical antiphase tilting of the  $O_6$  octahedra in the perovskite lattice. This mode is therefore associated with the zone boundary  $2\pi/a_{lat}$  ( $1/2, 1/2, 1/2$ )  $k$  point of the cubic first Brillouin zone, where  $a_{lat}$  is the lattice constant of the five-atom cubic perovskite cell. The second mode is more complex, as evidenced by the unusual pattern of lead and oxygen displacements shown in Figs. 1(a) and 1(b). It is labeled  $\Sigma_2$  and is associated with the  $2\pi/a_{lat}$  ( $1/4, 1/4, 0$ )  $k$  point. The anti-polar Pb motions in Fig. 1(a) are usually mentioned as the essential feature characterizing the PZO's antiferroelectric phase. (Here we use the terms antipolar and antiferroelectric indifferently. As regards the definition of antiferroelectrics, we adopt the one proposed in Ref. [13].) Finally, the  $Pbam$  ground state also presents a relatively small distortion inherent to a third, weaker soft mode; this final mode has  $S_4$  symmetry and is associated with the  $2\pi/a_{lat}$  ( $1/4, 1/4, 1/2$ ) wave vector [see Figs. 1(d)–1(f)].

Recent works [6–8] suggest that a trilinear coupling between the predominant  $R_4^+$ ,  $\Sigma_2$ , and the weaker  $S_4$  modes plays an important role to stabilize PZO's  $Pbam$  ground state. More precisely, first-principles calculations [6] show that, while the contribution of the trilinear term to the energy is relatively small—27 meV per formula unit (fu) out of the 392 meV/fu energy gain of the ground state with respect to the cubic high-symmetry phase—it is nevertheless critical for the AFE phase to prevail over competing polymorphs. Now,

while valuable, the existing theories have not addressed a critical, necessary ingredient for the preeminence of the  $Pbam$  phase, namely, the strongly unstable character of the exotic  $\Sigma_2$  mode, which accounts for about 250 meV/fu of the energy reduction. In this work, we reveal the atomistic couplings responsible for the occurrence of such an unusual structural instability.

Interestingly, such atomistic couplings exist in all perovskite compounds, and involve (anti)polar displacements of the  $A$  cations in the perovskite lattice (Pb in PZO's case) and rotations of the  $O_6$  octahedra. Remarkably, they can also explain and hold the key to understand many other nontrivial antipolar states (see, e.g., Refs. [14–16] and references therein) and even incommensurate phases [17,18] in various perovskites possessing a structural complexity that has acted as a major deterrent of detailed studies. In other words, the presently discovered couplings also provide an unified description of many antiferroelectric and incommensurate perovskites.

The manuscript is organized as follows. Section II describes these atomistic couplings, while Sec. III demonstrates their relevance to antiferroelectrics and incommensurate crystals. Section IV provides a further discussion that establishes, and compares with previous works, the analytical form that these atomistic couplings take in the continuum limit. Finally, Sec. V concludes this article.

**II. INTERATOMIC COUPLINGS**

Let us start by adopting the convention that the  $B$  cations of the  $ABO_3$  perovskite compounds are at the corners of the reference five-atom cell, the  $A$  cations being at the cell center. Let us denote by  $\mathbf{u}_i$  the vector representing the off-centering displacement of the  $A$  cation at cell  $i$  with respect to its ideal position in the cubic reference structure. For instance, the pattern of  $\mathbf{u}_i$ 's associated with the Pb displacements in the  $\Sigma_2$  mode of the AFE ground state of PZO is shown in Fig. 1(a). In that case, these  $\mathbf{u}_i$  vectors are either parallel or antiparallel to the pseudocubic  $[\bar{1}10]$  direction. Figure 1(a) further indicates that the  $\mathbf{u}_i$ 's in the  $\Sigma_2$  mode follow a “+ + —” pattern when

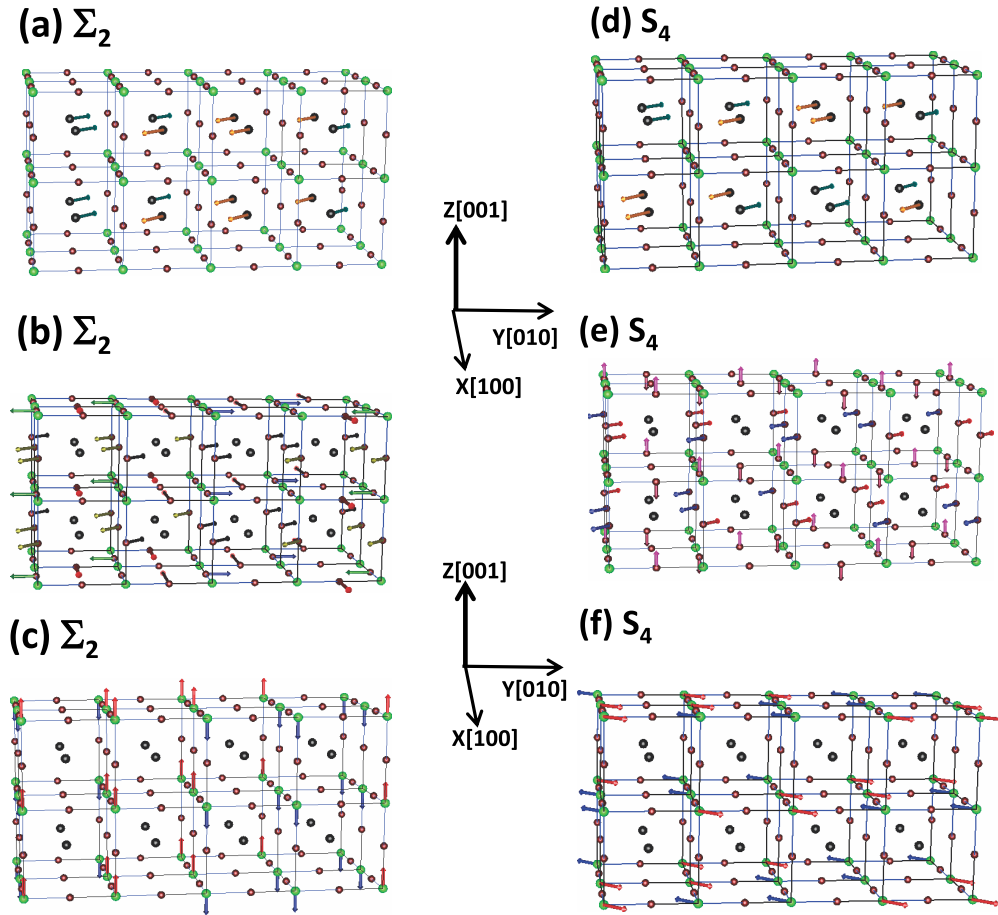


FIG. 1. Patterns of the  $A$ -cation distortions,  $\mathbf{u}_i$  (a), oxygen displacements (b) and corresponding  $B$ -centered oxygen octahedra rotation pseudovectors,  $\omega_i$  (c) for the  $\Sigma_2$  mode of  $ABO_3$  perovskites. (d)–(f) show the corresponding patterns but for the  $S_4$  mode. The  $A$ ,  $B$ , and  $O$  ions are shown by black, green, and red spheres, respectively. The different colors used for the arrows in each panel emphasize the different directions of the corresponding vectors.

one moves along the  $[100]$  or  $[010]$  pseudocubic directions in the  $(001)$  plane.

Let us also introduce a pseudovector  $\omega_i$  that characterizes the tilting of the oxygen octahedron centered at the  $B$  site in unit cell  $i$ . [Modes characterized by long-range ordered  $\omega_i$  tiltings are usually termed antiferrodistortive (AFD).] More precisely, the direction of  $\omega_i$  gives the axis about which the oxygen octahedron rotates and its magnitude yields the rotation angle [19]. It is important to realize that, by using the rotations of individual octahedra as independent variables, we can reproduce any rotational pattern, including cases in which the tiltings are *truncated* and the octahedra distort. To emphasize this point, Figure 1(b) displays the oxygen motions associated with the tilting of the oxygen octahedra in the  $\Sigma_2$  mode characterizing PZO's AFE; one can see that, out the four in-plane oxygen ions surrounding any  $B$  cation, only two move. Such distortions arise when the individual  $\omega_{i,z}$  rotations (about the  $z$  or  $[001]$  axis) display a “ $++--$ ” modulation pattern as we move along the in-plane  $[100]$  or  $[001]$  directions. Note that these AFD modes are qualitatively different from the *Glazer* rotational patterns [20] that are most usual in perovskites, which always involve “ $+ - + -$ ” (zone-boundary) modulations in the plane perpendicular to the rotation axis.

Interestingly, different types of energies coupling the  $\{\mathbf{u}_i\}$  and  $\{\omega_i\}$  variables have been reported in the literature. For example, biquadratic couplings (i.e., quadratic in both  $u$  and  $\omega$  variables) account for the well-known repulsion between polar and  $O_6$ -rotational distortions [19]. Additionally, coupling terms linear in  $u$  and either quadratic or cubic in  $\omega$  have been shown to yield collaborative effects involving both types of variables [21], as, e.g., in the so-called hybrid improper ferroelectrics [22–24]. Further, interactions that go as  $u^2\omega$  have been shown to be at the origin of inhomogeneous states and novel magnetoelectric effects [25]. However, none of these interaction terms can account for the occurrence of *hybrid* soft phonons like PZO's  $\Sigma_2$  mode. Indeed, in that case, we need to explore the possibility that the polar and rotational variables couple at the harmonic level, a question that, as far as we know, has never been discussed in the literature on perovskites. Notably, model studies for perovskites in which both distortion types are relevant have either focused on the effects associated with the anharmonic couplings [26] or even assumed that local dipoles and  $O_6$  rotations are decoupled harmonically [27]. It is thus worth to emphasize that there is no fundamental (symmetry) reason for such modes to not interact at the harmonic level, and that such a feature constitutes an approximation in most existing models.

Here, we set up to identify the simplest  $\mathcal{O}(u\omega)$  couplings that may potentially lead to *hybrid* phonons as PZO's  $\Sigma_2$  and  $S_4$  modes. The simplest (in the sense that it involves relatively close neighbors) interaction that we found has the form:

$$\Delta E = \mathcal{K} \sum_i \sum_{l,m,n=0,1} \sum_{\alpha,\beta,\gamma=x,y,z} \epsilon_{\alpha\beta\gamma} u_{i,\alpha} \omega_{ilmn,\beta} (-1)^{(lx+my+nz)_\gamma}, \quad (1)$$

where  $\mathcal{K}$  is a material-dependent constant that characterizes the strength of this coupling. The sum over  $i$  runs over all the five-atom cells of the perovskite structure, and the  $x$ ,  $y$ , and  $z$  subscripts denote the Cartesian components of the  $\mathbf{u}_i$  vectors and  $\omega_i$  pseudovectors—with the  $x$ ,  $y$ , and  $z$  axes being chosen along the pseudocubic [100], [010], and [001] directions, respectively.  $\omega_{ilmn}$  (with  $l,m,n = 0$  or  $1$ ) represents the rotation of the  $O_6$  group in the cell that is reached from  $i$  by following the lattice vector  $\mathbf{R}_{ilmn} = a_{\text{lat}}(lx + my + nz)$ .  $(lx + my + nz)_\gamma$  is the  $\gamma$  component of the vector in parenthesis. Finally,  $\epsilon_{\alpha\beta\gamma}$  is the Levi-Civita symbol, i.e., it equals 1 when the ordered triad  $\alpha\beta\gamma$  forms a right-handed system,  $-1$  when left-handed, and 0 when there are repeated indexes. Figure 2 schematizes coupling terms inherent to Eq. (1).

Let us now consider distortions given by

$$\begin{aligned} u_{i,\alpha} &= A_\alpha \{\exp[i(\mathbf{k}_\alpha \cdot \mathbf{R}_i + \phi_\alpha)] + \text{c.c.}\}, \\ \omega_{i,\alpha} &= A'_\alpha \{\exp[i(\mathbf{k}'_\alpha \cdot \mathbf{R}_i + \phi'_\alpha)] + \text{c.c.}\}, \end{aligned} \quad (2)$$

where  $\mathbf{R}_i$  is the lattice vector corresponding to cell  $i$  and  $\alpha = x, y, z$ . The  $\mathbf{k}_\alpha$  wave vectors characterize the spatial modulation of each of the components of the  $\mathbf{u}_i$  vectors. Similarly, the  $\mathbf{k}'_\alpha$  vectors define, in direction and length, the modulated distortions of the Cartesian components of the  $\omega_i$  pseudovectors. The  $A_\alpha$  and  $A'_\alpha$  scalars quantify the magnitude of the  $u$  and  $\omega$  distortions, respectively, and are taken to be real. The  $\phi_\alpha$  and  $\phi'_\alpha$  angles are phases characterizing specific  $u$  and  $\omega$  patterns, respectively.

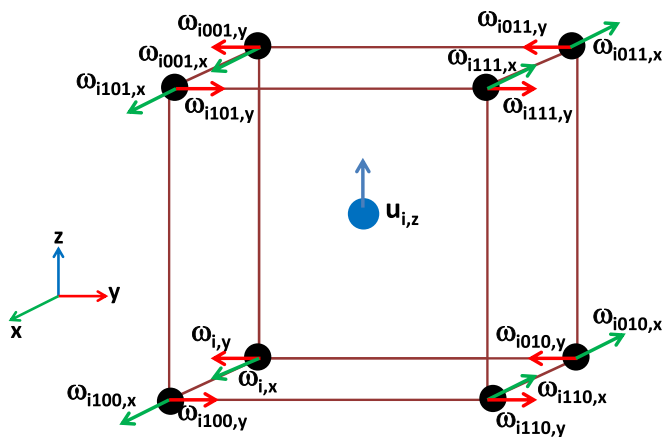


FIG. 2. Sketch of representative coupling terms in  $\Delta E$  of Eq. (1). Only the couplings involving  $u_{i,z}$  are schematized here, since the remaining terms can be straightforwardly derived from the ones shown by applying the symmetry elements of the cubic  $Pm\bar{3}m$  space group. The blue arrow on the central A cation stands for the  $u_{i,z}$  displacement. The green and red arrows on the corner B cations represent the  $x$  and  $y$  components, respectively, of the  $\omega$  pseudovectors.

By inserting Eqs. (2) into Eq. (1), we can identify which combinations of  $\mathbf{k}_\alpha$  and  $\mathbf{k}'_\alpha$  wave vectors result in an interaction via this new coupling. Hence the expression for the energy can be rewritten as

$$\begin{aligned} \frac{\Delta E}{\mathcal{K}} &= \sum_{\alpha,\beta=x,y,z} A_\alpha A'_\beta \sum_{\mathbf{G}} [f_{\alpha\beta} \delta(\mathbf{G} - \mathbf{k}_\alpha - \mathbf{k}'_\beta) \\ &+ f_{\alpha\beta}^* \delta(\mathbf{G} + \mathbf{k}_\alpha + \mathbf{k}'_\beta) \\ &+ g_{\alpha\beta} \delta(\mathbf{G} + \mathbf{k}_\alpha - \mathbf{k}'_\beta) + g_{\alpha\beta}^* \delta(\mathbf{G} - \mathbf{k}_\alpha + \mathbf{k}'_\beta)], \end{aligned} \quad (3)$$

where  $\delta$  is the Dirac delta function and  $\mathbf{G}$  runs over the reciprocal lattice vectors corresponding to the five-atom cubic perovskite structure. The  $f_{\alpha\beta}$  and  $g_{\alpha\beta}$  coefficients are given by

$$f_{\alpha\beta} = \exp[i(\phi_\alpha + \phi'_\beta)] a_{\alpha\beta} \quad (4)$$

and

$$g_{\alpha\beta} = \exp[i(-\phi_\alpha + \phi'_\beta)] a_{\alpha\beta}, \quad (5)$$

where

$$a_{\alpha\beta} = \sum_{\eta=x,y,z} \epsilon_{\alpha\beta\eta} \prod_{\gamma=x,y,z} [1 + (-1)^{\delta_{\gamma\eta}} \exp(ik'_{\beta,\gamma} a_{\text{lat}})] \quad (6)$$

with  $\delta_{\gamma\eta}$  being the Kronecker  $\delta$  and  $k'_{\beta,\gamma}$  the  $\gamma$  component of the  $\mathbf{k}'_\beta$  vector.

### III. APPLICATIONS OF THE INTERATOMIC COUPLINGS

Having introduced the basic equations for this new coupling energy, let us inspect what the implications are as regards the possible occurrence of AFE and other complex instabilities in perovskite lattices. More precisely, we will consider a number of complex distortion patterns and show that they lead to reduction of the energy of the cubic perovskite phase via the new interaction term.

#### A. The $\Sigma_2$ antiferroelectric mode

Let us first consider the case of  $\mathbf{k}_x = \mathbf{k}_y = \frac{\pi}{2a_{\text{lat}}}(\mathbf{x} + \mathbf{y})$ . The Dirac functions of the type  $\delta(\mathbf{G} - \mathbf{k}_\alpha - \mathbf{k}'_\beta)$  in Eq. (3) imply that for  $\mathbf{k}'_\beta = -\mathbf{k}_\alpha = -\mathbf{k}_y$ , we can, in principle, have interactions contributing to  $\frac{\Delta E}{\mathcal{K}}$ . Now, it is immediate to see from Eq. (6) that  $a_{xy} = a_{yx} = 0$  for this choice of wave vectors. (We also trivially have  $a_{xx} = a_{yy} = 0$ .) Nevertheless, we do have a nonvanishing result when we consider  $\mathbf{k}'_z = -\mathbf{k}_x = -\mathbf{k}_y$ . For such a  $k'$  point we can prove that  $a_{xz}$  and  $a_{yz}$  are finite and Eq. (3) becomes

$$\frac{\Delta E(\Sigma_2)}{\mathcal{K}} = -8A_x A'_z \cos(\phi_x + \phi'_z) + 8A_y A'_z \cos(\phi_y + \phi'_z). \quad (7)$$

Further, it is clear from Eq. (7) that the interaction is maximized in specific cases; for example, when both  $\phi_x + \phi'_z$  and  $\phi_y + \phi'_z$  take values of the form  $\pi n$ , with  $n \in \mathbb{Z}$ , provided  $A_x$  and  $A_y$  have opposite signs.

For instance, we get a maximum coupling for  $\phi_x = \phi_y = -\frac{3\pi}{4}$  and  $\phi'_z = -\frac{\pi}{4}$ . In that case, the A-cation displacements are out-of-phase with respect to the AFD distortions by  $90^\circ$  (since  $\phi'_z - \phi_x = \frac{\pi}{2}$ ), and the resulting patterns for the  $u$  and  $\omega$  distortions are exactly those shown in Figs. 1(a) and 1(c), respectively, which correspond to the soft  $\Sigma_2$  phonon mode

in PZO, i.e. they are of the form “+ + --”. Therefore the coupling in Eq. (1) naturally explains the exotic character of the AFE order in PZO and other materials that share similar features (e.g., PbHfO<sub>3</sub> or PHO [12,28]).

It is also interesting to realize that maximizing the interaction in Eq. (7) can also lead to solutions that are *not* those associated with PZO’s AFE pattern. For example, if we choose  $\phi_x = \phi_y = \phi'_z = -\frac{\pi}{2}$ , we have a second solution that has exactly the same energy,  $\mathcal{K}(8A_x A'_z - 8A_y A'_z)$ , as the first case discussed above. However, this alternative choice yields a rather different pattern for the A-cation displacements and oxygen octahedral tiltings. More specifically, Eqs. (2) correspond to “0 + 0–” modulations in which positive and negative values of the  $u$  and  $\omega$  vectors intercalate with null distortions as we move along any of the three Cartesian axis. Note that these two “+ + --” and “0 + 0–” cases are indistinguishable (i.e., perfectly degenerate) at the harmonic level. The fact that materials like PZO and PHO adopt the former pattern over the latter is, in fact, related to anharmonic couplings involving local dipoles and tiltings, and in particular to energies of the form  $\alpha_u \sum_i (u_{i,x}^2 + u_{i,y}^2 + u_{i,z}^2)^2$  and  $\alpha_\omega \sum_i (\omega_{i,x}^2 + \omega_{i,y}^2 + \omega_{i,z}^2)^2$ , where  $\alpha_u$  and  $\alpha_\omega$  are positive constants and where  $i$  runs over all the sites. As a matter of fact, such energies are higher in the “0 + 0–” pattern than in the “+ + --” case because the “+” and “–” displacements in the “0 + 0–” modulation are larger by a factor of  $\sqrt{2}$  in magnitude than the “+” and “–” displacements in the “+ + --” pattern (when the “+ + --” and “0 + 0–” waves of Eq. (2) have the same  $A_\alpha$  and  $A'_\alpha$  amplitudes).

### B. The $S_4$ antiferroelectric mode

Let us now consider the case of the  $S_4$  mode, which is also known to contribute to the  $Pbam$  ground state of PZO and PHO [6–9,12]. The corresponding patterns for the  $u$ ’s, oxygen atomic motions and  $\omega$ ’s are shown in Figs. 1(d), 1(e), and 1(f), respectively. For such mode, we choose  $\mathbf{k}_x = \mathbf{k}_y = \frac{\pi}{2a_{\text{lat}}}(\mathbf{x} + \mathbf{y}) + \frac{\pi}{a_{\text{lat}}}\mathbf{z}$  in Eq. (2). Then, it can be checked that in this case we have nonvanishing interactions for  $\mathbf{k}'_x = \mathbf{k}'_y = -\mathbf{k}_x = -\mathbf{k}_y$  via the  $\delta(\mathbf{G} - \mathbf{k}_\alpha - \mathbf{k}'_\beta)$  in Eq. (3). The resulting  $\Delta E/\mathcal{K}$  solely involves the  $a_{xy}$  and  $a_{yx}$  terms defined in Eq. (6) and becomes

$$\frac{\Delta E(S_4)}{\mathcal{K}} = 8A_x A'_y \sin(\phi_x + \phi'_y) - 8A_y A'_x \sin(\phi_y + \phi'_x). \quad (8)$$

The magnitude of the interaction is thus maximized for  $\phi_x + \phi'_y = \phi_y + \phi'_x = \frac{\pi}{2} + \pi n$ , where  $n \in \mathbb{Z}$ , if  $A_x A'_y$  and  $A_y A'_x$  have opposite signs. One such solution is  $\phi_x = \phi_y = -\frac{\pi}{4}$  and  $\phi'_x = \phi'_y = \frac{3\pi}{4}$ , which yields the patterns of  $f$  A-cation displacements and tiltings shown in Figs. 1(d) and 1(f), respectively. Hence, the coupling of Eq. (1) can also explain the complex atomic distortion associated with the soft  $S_4$  mode of PZO and PHO.

### C. The $\Lambda_3$ symmetry antiferroelectric mode

Let us now consider other complex atomic patterns as those displayed in Fig. 3. Such patterns have been demonstrated to contribute to a stable and complex antipolar  $Pnma$  structure in BiFeO<sub>3</sub> and BiFe<sub>1/2</sub>Sc<sub>1/2</sub>O<sub>3</sub> [15,16], involving a cell that

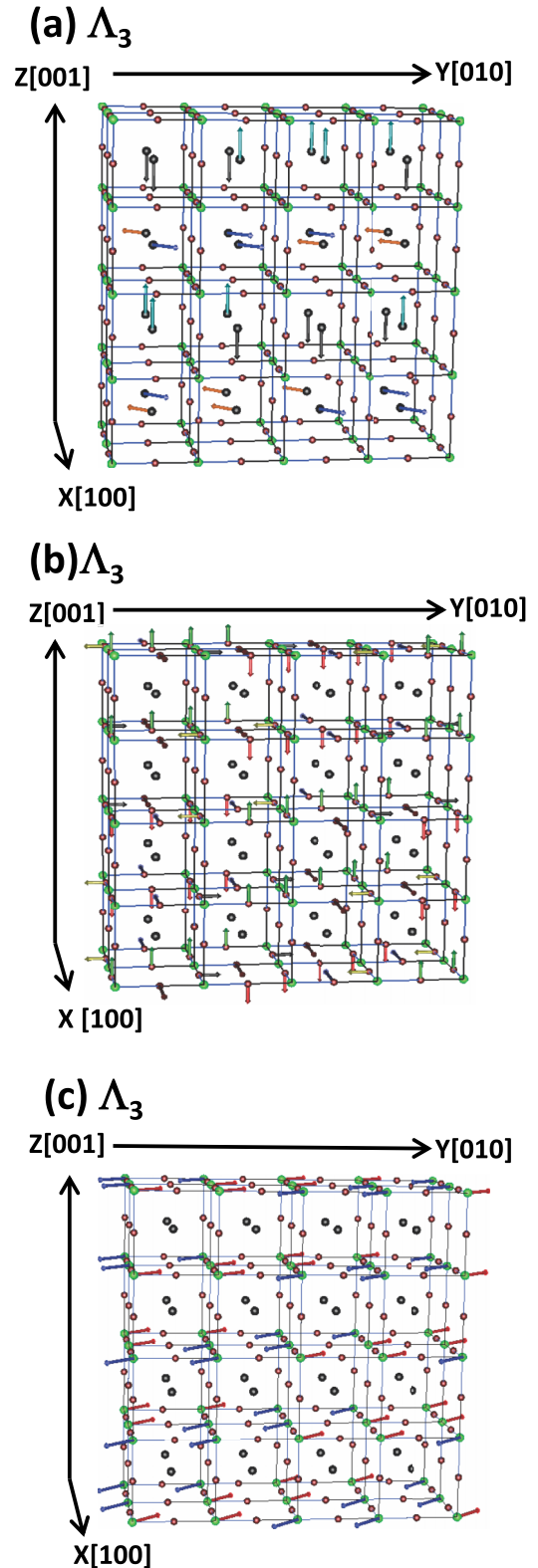


FIG. 3. Same as Figs. 1(a)–1(c) but for the  $\Lambda_3$  modes of  $ABO_3$  perovskites.

is a  $\sqrt{2} \times 4 \times 2\sqrt{2}$  multiple of the five-atom perovskite unit, and are associated with  $\Lambda_3$  modes. As shown in Fig. 3(a), the  $x$  and  $y$  components of the A-cation displacements can be described by  $u_{i,x} = u_{i,y} = A \cos(\{\mathbf{k}_{1x} \cdot \mathbf{R}_i + \phi_x\}) +$

$A \cos(\{\mathbf{k}_{2x} \cdot \mathbf{R}_i + \phi_x\})$ , with  $\phi_x = \frac{\pi}{4}$ ,  $\mathbf{k}_{1x} = \frac{\pi}{2a_{\text{lat}}}(\mathbf{x} + \mathbf{y} + \mathbf{z})$ , and  $\mathbf{k}_{2x} = \frac{\pi}{2a_{\text{lat}}}(\mathbf{x} + \mathbf{y} - \mathbf{z})$ . In other words, and as consistent with Ref. [16], two different  $k$ -vectors (related by symmetry, but not by inversion) are needed to describe such waves. Similarly, Fig. 3(a) further shows that  $u_{i,z} = C \cos(\{\mathbf{k}_{1x} \cdot \mathbf{R}_i + \phi_z\}) - C \cos(\{\mathbf{k}_{2x} \cdot \mathbf{R}_i + \phi_z\})$ , with  $\phi_z = -\frac{3\pi}{4}$ . Figure 3(c) also tells us that the  $x$ - and  $y$ -components of the  $\omega$ 's are activated in this mode, while the  $z$  component is null; we thus have  $\omega_{i,x} = -\omega_{i,y} = A' \cos(\{-\mathbf{k}_{1x} \cdot \mathbf{R}_i + \phi'_{1x}\}) + A' \cos(\{-\mathbf{k}_{2x} \cdot \mathbf{R}_i + \phi'_{2x}\})$ , with  $\phi'_{1x} = 0$  and  $\phi'_{2x} = \frac{\pi}{2}$ . It is straightforward to generalize Eq. (2) to the case of a superposition of two waves with different  $k$  vectors (using these new  $A$ ,  $C$  and  $A'$  coefficients), and then insert it in Eq. (1), to yield the following nonvanishing  $\Delta E$ :

$$\begin{aligned}
 \frac{\Delta E(\Lambda_3)}{\mathcal{K}} &= 8CA'[\cos(\phi_z + \phi'_{1x}) + \sin(\phi_z + \phi'_{1x}) \\
 &\quad - \cos(\phi_z + \phi'_{2x}) + \sin(\phi_z + \phi'_{2x})] \\
 &\quad - 8AA'[\cos(\phi_x + \phi'_{1x}) + \sin(\phi_x + \phi'_{1x}) \\
 &\quad - \cos(\phi_x + \phi'_{2x}) + \sin(\phi_x + \phi'_{2x})] \\
 &= -16\sqrt{2}(CA' + AA'). \tag{9}
 \end{aligned}$$

It is thus clear that the bi-linear coupling of Eq. (1) can also explain the occurrence of the atomic patterns displayed in Fig. 3.

#### D. Modes along the $\Sigma$ line

Let us now consider the case in which  $\mathbf{k}_x = \mathbf{k}_y$  correspond to a wave vector along the  $\Sigma$  line that connects the center of the first Brillouin zone with the boundary  $M$ -point given by  $\pi/a_{\text{lat}}(\mathbf{x} + \mathbf{y})$ . We thus have  $\mathbf{k}_x = \mathbf{k}_y = \lambda\pi/a_{\text{lat}}(\mathbf{x} + \mathbf{y})$ , where  $\lambda$  is a real number between 0 and 1. We find that in this case Eq. (3) reduces to

$$\begin{aligned}
 \frac{\Delta E(\Sigma)}{\mathcal{K}} &= 8 \sin(\lambda\pi)[A_x A'_z \sin(\phi_x + \phi'_z - \lambda\pi) \\
 &\quad - A_y A'_z \sin(\phi_y + \phi'_z - \lambda\pi)]. \tag{10}
 \end{aligned}$$

Several important conclusions can be drawn from this result. First, the  $\sin(\pi\lambda)$  function in Eq. (10) automatically implies that the effect of our new coupling is null at the  $\Gamma$  ( $\lambda = 0$ ) and  $M$  ( $\lambda = 1$ ) points. In contrast, the modes associated with intermediate  $k$  points along the  $\Sigma$  line are affected by the new coupling. Note that such a coupling could thus explain modulations of the  $O_6$  rotations as those discussed in Ref. [30] in Li-doped  $\text{NdTiO}_3$ , provided that they are accompanied by  $A$ -cation displacements. Second, for any selected  $k$  point in the  $\Sigma$  line, the magnitude of the coupling is maximum when  $\phi_x + \phi'_z$  and  $\phi_y + \phi'_z$  take values of the form  $\pi/2 + \lambda\pi + \pi n$ , where  $n \in \mathbb{Z}$ , provided that  $A_x$  and  $A_y$  have opposite signs. Third, it is important to realize that *nonrational* values of  $\lambda$  can also yield a coupling energy, i.e., our new interaction can potentially be the driving force for the formation of *incommensurate* perovskite phases.

#### E. Phonon spectra and incommensurability

Let us now discuss how our new coupling energy affects the phonon bands of a perovskite material. To do this, we

consider the ideal cubic structure and assume that the second derivatives of the energy (at the harmonic level) with respect to the atomic displacements associated with the polar distortions and octahedral rotations are given by

$$\begin{aligned}
 E''_u(\lambda) &= \frac{\partial^2 E}{\partial u(\lambda)^2} = F_u + G_u \cos(\lambda\pi), \\
 E''_\omega(\lambda) &= \frac{\partial^2 E}{\partial \omega(\lambda)^2} = F_\omega + G_\omega \cos(\lambda\pi), \tag{11} \\
 E''_{u\omega}(\lambda) &= \frac{\partial^2 E}{\partial u(\lambda)\partial \omega(\lambda)} = H_{u\omega} \sin(\lambda\pi),
 \end{aligned}$$

where, as before, we use  $\lambda$  to label  $k$  points in the  $\Sigma$  line [31]. The diagonal terms of this  $k$ -dependent Hessian matrix represent the typical energetics of polar and AFD bands in perovskites. The off-diagonal elements have the form of the coupling that we are introducing in this work, as it is derived from Eq. (10) by taking  $\sin(\phi_x + \phi'_z - \lambda\pi) = \sin(\phi_y + \phi'_z - \lambda\pi) = 1$ . The  $F$ ,  $G$ , and  $H$  parameters characterize the energetics of the  $u$  and  $\omega$  variables and their mutual coupling [the  $H_{u\omega}$  coefficient is therefore related to the  $\mathcal{K}$  parameter of Eq. (1)]. Diagonalizing this  $k$ -dependent Hessian results in two bands that are given by

$$\begin{aligned}
 \kappa_-(\lambda) &= \frac{E''_u(\lambda) + E''_\omega(\lambda)}{2} \\
 &\quad - \frac{\sqrt{(E''_u(\lambda) - E''_\omega(\lambda))^2 + 4H_{u\omega}^2 \sin^2(\lambda\pi)}}{2}, \\
 \kappa_+(\lambda) &= \frac{E''_u(\lambda) + E''_\omega(\lambda)}{2} \\
 &\quad + \frac{\sqrt{(E''_u(\lambda) - E''_\omega(\lambda))^2 + 4H_{u\omega}^2 \sin^2(\lambda\pi)}}{2}. \tag{12}
 \end{aligned}$$

These two bands are associated with eigenvectors that display a hybrid  $u$ - $\omega$  character at all  $k$  points except for the  $\lambda = 0$  and  $\lambda = 1$  limits. The degree of hybridization depends on the relative magnitude of the coupling parameter  $H_{u\omega}$ . Note also that, whenever we have negative eigenvalues  $\kappa_-$  or  $\kappa_+$ , the corresponding eigenvector constitutes an instability of the cubic perovskite structure.

Let us consider two choices of parameters and thus discuss the phenomenology that our simple model can yield. Figures 4(a)–4(c) illustrate the situation for a case (1) characterized by the following features: (i)  $E''_u(\lambda)$  is lowest at  $\Gamma$  and rapidly increases with  $\lambda$  (i.e., we have a strong ferroelectric instability of displacive character); (ii)  $E''_\omega(\lambda)$  is minimal at the  $M$  point (i.e., we have a strong AFD instability) and rapidly increases for decreasing  $\lambda$ ; and (iii) the minimum of  $E''_\omega(\lambda)$  is lower than the minimum of  $E''_u(\lambda)$  (i.e., the AFD instability is stronger than the ferroelectric one). Figures 4(a)–4(c) further display the resulting  $\kappa_-(\lambda)$  and  $\kappa_+(\lambda)$  eigenvalues of Eq. (12) for three different choices of the  $H_{u\omega}$  coupling parameter. Moreover, Fig. 4(d) shows the dependency on  $H_{u\omega}$  of the value of  $\lambda$  at which  $\kappa_-(\lambda)$  is minimum, which we denote as  $\lambda_{\text{min}}$ . Figure 4(a) indicates that a relatively small  $H_{u\omega}$  results in a small gap between the  $\kappa_-(\lambda)$  and  $\kappa_+(\lambda)$  bands. Note that the associated eigenvectors change character as a function of  $\lambda$ . Thus, for example, the distortion mode associated with

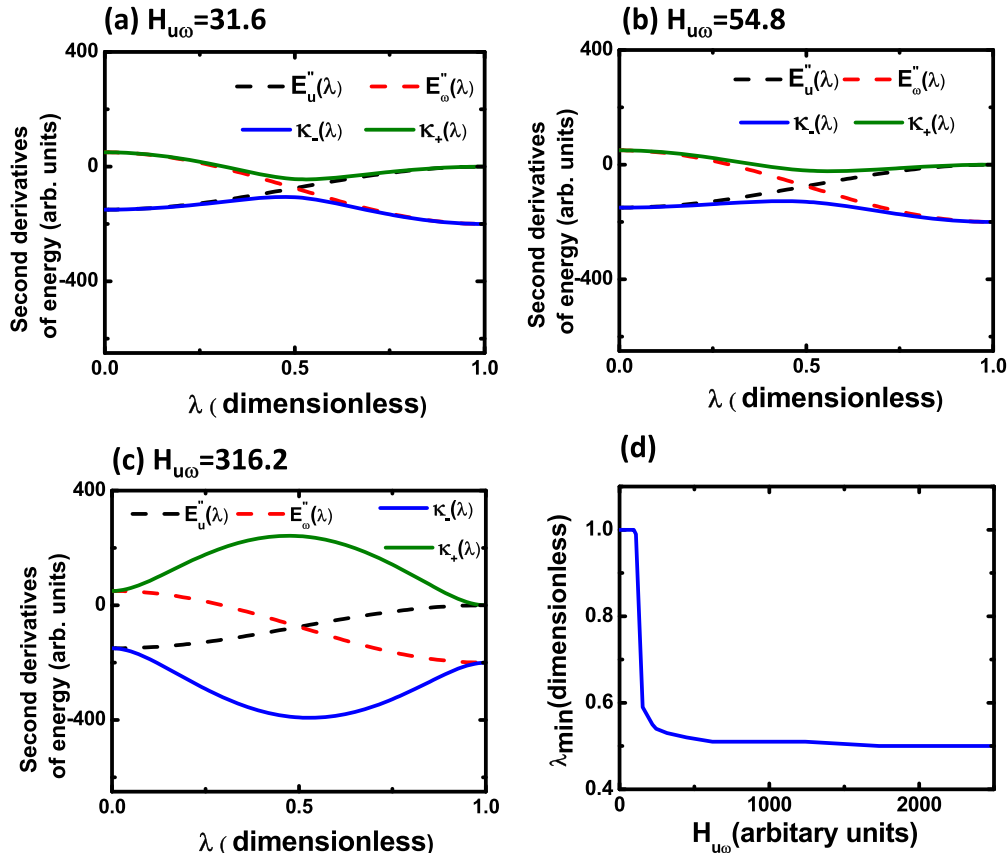


FIG. 4. Dependencies of  $E''_u(\lambda)$ ,  $E''_\omega(\lambda)$ ,  $\kappa_-(\lambda)$ , and  $\kappa_+(\lambda)$  along the  $\Sigma$  line, choosing here (in arbitrary units)  $E''_u(\lambda) = -75 - 75 \cos(\pi\lambda)$  and  $E''_\omega(\lambda) = -75 + 125 \cos(\pi\lambda)$ .  $\kappa_-(\lambda)$  and  $\kappa_+(\lambda)$  are given by Eq. (12) for three different cases:  $H_{u\omega} = 31.6$  (a), 54.8 (b), and 316.2 (c). (d) further displays the  $\lambda_{\min}$  value of  $\lambda$  at which  $\kappa_-(\lambda)$  is minimum, as a function of  $H_{u\omega}$ .

the smaller eigenvalue  $\kappa_-$  is strongly polar close to  $\Gamma$  [with  $\kappa_-(\lambda \approx 0) \sim E''_u(\lambda \approx 0)$ ], but it is rotational-like close to  $M$  [with  $\kappa_-(\lambda \approx 1) \sim E''_\omega(\lambda \approx 1)$ ]. Such features are typical of an avoided crossing (anticrossing) between bands, as we have in this case. As  $H_{u\omega}$  grows [Fig. 4(b)], we find that  $\kappa_-(\lambda)$  is rather insensitive to  $\lambda$  for a large region around  $\lambda = 1/2$ . Furthermore and as shown in Fig. 4(d),  $\lambda_{\min}$  moves away from the value of 1 when  $H_{u\omega}$  is above a critical value [as it is straightforward to analytically prove when considering Eqs. (11) and (12)]. It then rapidly converges to  $\lambda_{\min} = 1/2$  [see Fig. 4(c)] when further increasing  $H_{u\omega}$ , i.e., the dominant instability is a mode with hybrid  $u - \omega$  character for large enough  $H_{u\omega}$ .

These results are reminiscent of what was found for the phonons of cubic PZO along the  $\Sigma$  line, as computed from first principles [32]. More specifically, PZO seems to correspond to the case shown in Fig. 4(b), for intermediate values of the  $u - \omega$  coupling. Indeed, PZO presents soft  $\Sigma$  modes with a hybrid character, associated with a very flat band; yet, the dominant instability of the cubic phase is the AFD one at the boundary of the Brillouin zone. (More precisely, PZO displays a very flat branch of AFD-like phonons connecting the  $M$  and  $R$   $k$  points [6], where  $\mathbf{k}_R = \pi/a_{\text{lat}}(\mathbf{x} + \mathbf{y} + \mathbf{z})$ ). Hence, at the harmonic level, we would predict PZO to present a regular AFD ground state, as opposed to the AFE one it actually displays. Indeed, as demonstrated in Ref. [6], the additional factor that permits the stabilization of PZO's AFE phase is the trilinear coupling between  $R_4^+$ ,  $\Sigma_2$ , and  $S_4$ .

Let us now tackle case (2) that corresponds to a different choice of parameters and yields the results shown in Fig. 5. In case (2), the  $E''_u(\lambda)$  still has a minimum at  $\lambda = 0$  but its dependence with  $\lambda$  is relatively weak (i.e., we have a ferroelectric instability that tends to be of the order-disorder type). Further, this minimum of  $E''_u(\lambda)$  is only slightly higher than the  $M$ -point minimum of  $E''_\omega(\lambda)$ . Figures 5(a)–5(c) depict  $E''_u(\lambda)$  and  $E''_\omega(\lambda)$ , along with the coupled  $\kappa_-$  and  $\kappa_+$  eigenvalues, for increasing magnitude of the coupling coefficient  $H_{u\omega}$ . One can see that the minimum of  $\kappa_-(\lambda) = \kappa_-(\lambda_{\min})$  is displaced from the  $M$  point towards  $\lambda = 1/2$  as  $H_{u\omega}$  increases above a certain value. This is because the minimum of  $\kappa_-(\lambda)$  corresponds to the minimum of  $E''_\omega(\lambda)$ , that is  $\lambda = 1$ , for small  $H_{u\omega}$ , while the cross-coupling  $E''_{u\omega}(\lambda)$  of Eq. (11) always favors the minimum of  $\kappa_-(\lambda)$  to be at  $\lambda = 1/2$  for arbitrarily large  $H_{u\omega}$ .  $\lambda_{\min}$  therefore possesses different values, depending on the strength of  $H_{u\omega}$ , with these values being not necessarily inverse of integers. For instance, as also seen in Fig. 5(b),  $\lambda_{\min}$  is equal to 0.69 for  $H_{u\omega} = 54.8$  (note that this value of  $H_{u\omega}$  rather yields, in Fig. 4(b) [i.e., in case (1)], a  $\kappa_-(\lambda)$  having a minimum at the  $M$  point, i.e., at  $\lambda = 1$ ). In other words, the dominant instability of our model may correspond to arbitrary long-range, even *incommensurate*, distortions of the perovskite lattice [33], with the period of incommensurate distortions being dependent on the coupling coefficient  $\mathcal{K}$  of Eq. (1). Let us stress that the incommensurate distortion involves both the  $A$ -cation displacements and AFD motions,

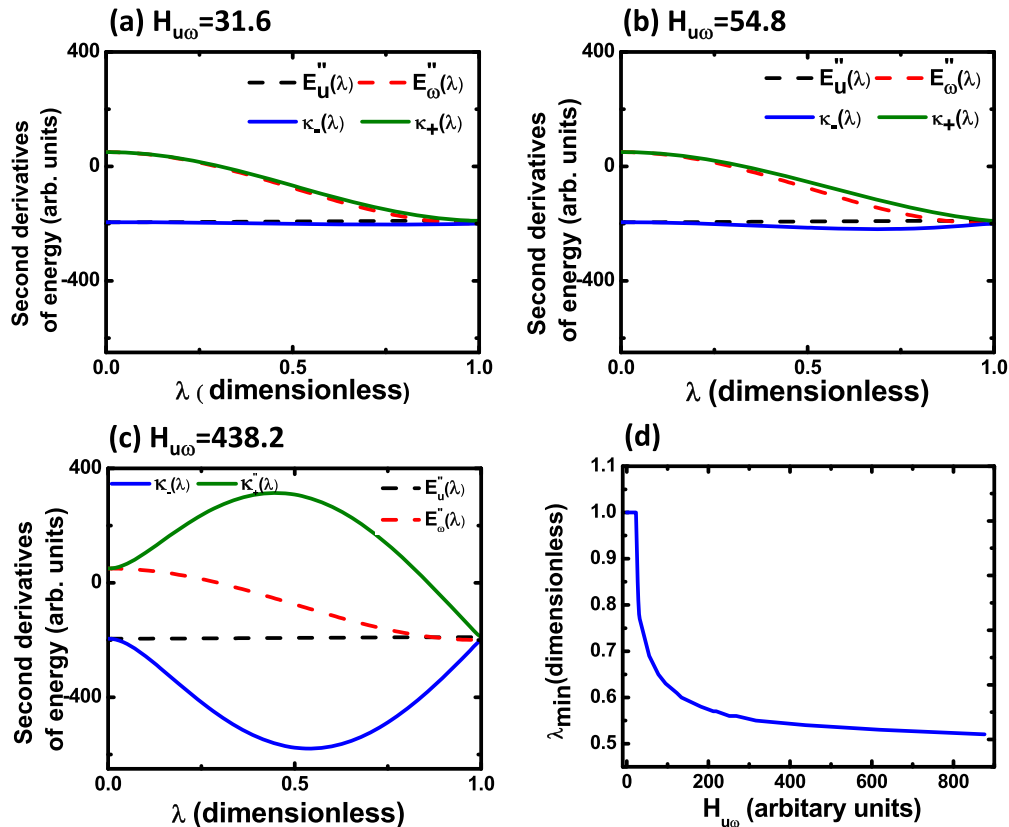


FIG. 5. Dependencies of  $E_u''(\lambda)$ ,  $E_\omega''(\lambda)$ ,  $\kappa_-(\lambda)$ , and  $\kappa_+(\lambda)$  along the  $\Sigma$  line, choosing here (in arbitrary units)  $E_u''(\lambda) = -192.5 - 2.5 \cos(\pi\lambda)$  and  $E_\omega''(\lambda) = -75 + 125 \cos(\pi\lambda)$ .  $\kappa_-(\lambda)$  and  $\kappa_+(\lambda)$  are given by Eq. (12) for three different cases:  $H_{u\omega} = 31.6$  (a), 54.8 (b), and 438.2 (c). (d) further displays the  $\lambda_{\min}$  value of  $\lambda$  at which  $\kappa_-(\lambda)$  is minimum, as a function of  $H_{u\omega}$ .

since the eigenvector corresponding to  $\kappa_-(\lambda)$  combines both features. The results of this analysis are thus reminiscent of the Neutron-Rietveld refinement of the incommensurate phase of the  $\text{Pb}(\text{Co,W})\text{O}_3$  compound, which was described as presenting both significant shifts of the Pb atoms and a rather complex mixing of tilt and deformation of the oxygen octahedra [17].

#### IV. DISCUSSION

Our prediction that nonperiodic structures can arise from the (microscopic) coupling between polar and rotational variables bears a strong resemblance with the (phenomenological) theory proposed by Heine and McConnell (HM) [35], which is based on the coupling between two different modes of transformation. More precisely, these authors worked with two modes denoted as  $\psi$  and  $\varphi$ , which they considered to be coupled by the interaction energy

$$\Delta E_{\text{int}}^{\text{HM}} = h(\varphi \nabla \psi - \psi \nabla \varphi), \quad (13)$$

where  $h$  is a constant and  $\nabla$  the gradient operator in one dimension. Note that the right-hand side of Eq. (13) is a Lifshitz invariant [36], and has also been used in other phenomenological approaches to incommensurate crystals [37].

It is interesting to determine the form that our microscopic coupling in Eq. (1) takes in the continuum limit, in order to (i) check whether it is similar to Eq. (13) that was previously proposed in Refs. [35,37] and (ii) have an expression that can

be used in the development of phenomenological theories. Indeed, if we focus on the terms involving a certain  $\mathbf{u}_i$  in our Eq. (1), it is apparent that this quantity is coupled to the spatial derivatives of  $\omega_i$ . More precisely, if we take  $\mathbf{u}$  and  $\omega$  to be the continuum limit of our local dipoles and  $\text{O}_6$  rotations, we can see that Eq. (1) can be rewritten as  $\sim \mathbf{u} \cdot (\nabla \times \omega)$ . Alternatively, the microscopic Eq. (1) can equally be rewritten by choosing a specific  $\omega_i$  at a given  $B$ -site  $i$  and considering its coupling with the spatial derivatives of the  $u$  displacements. In that case, the continuum limit goes as  $\sim \omega \cdot (\nabla \times \mathbf{u})$ . It is therefore more elegant to adopt the following form for the continuum version of Eq. (1):

$$\Delta E_{\text{cont}} = \frac{\mathcal{K}}{2} [\mathbf{u} \cdot (\nabla \times \omega) + \omega \cdot (\nabla \times \mathbf{u})]. \quad (14)$$

Equation (14) therefore contains a term of the form  $(u_x \frac{\partial \omega_z}{\partial y} - \omega_z \frac{\partial u_x}{\partial y})$ , that is similar to the previously suggested Eq. (13) when choosing  $\varphi = u_x$ ,  $\psi = \omega_z$  and taking the gradient to be the partial derivative with respect to  $y$ . However, Eq. (14) is more general than the interaction proposed by Heine and McConnell, since it contains five other, symmetry-equivalent terms, namely,  $(-u_y \frac{\partial \omega_z}{\partial x} + \omega_z \frac{\partial u_y}{\partial x})$ ,  $(-u_x \frac{\partial \omega_y}{\partial z} + \omega_y \frac{\partial u_x}{\partial z})$ ,  $(u_y \frac{\partial \omega_x}{\partial z} - \omega_x \frac{\partial u_y}{\partial z})$ ,  $(u_z \frac{\partial \omega_y}{\partial x} - \omega_y \frac{\partial u_z}{\partial x})$ , and  $(-u_z \frac{\partial \omega_x}{\partial y} + \omega_x \frac{\partial u_z}{\partial y})$ . In fact, the general form of Eq. (14), that involves the sum of (i) a dot product between a first vector, which is polar and the curl of the second vector, which is axial, and (ii) another dot product that is now between the second

vector and the curl of the first vector, constitutes an energy invariant that has never been previously proposed to the best of our knowledge, while being perfectly valid on symmetry and physical considerations.

We also performed first-principles calculations to extract the  $\mathcal{K}$  coefficient of two different materials, namely,  $\text{PbZrO}_3$  and  $\text{CaTiO}_3$ , that exhibit similar Goldschmidt tolerance factor [29]. For that, we chose the configurations of oxygen octahedral tiltings depicted in Fig. 1(b) and collected the force acting on the  $A$  atoms as a function of the magnitude of oxygen octahedral tiltings [these configurations are thus associated with the  $2\pi/a_{\text{lat}}$  (1/4, 1/4, 0)  $k$  point and possess  $A$  and  $B$  cations sitting at their ideal positions]. Equation (1) tells us that such force should be linearly dependent on this magnitude, with the resulting slope being directly proportional to the  $\mathcal{K}$  coefficient. These first-principles calculations did confirm such linearity, and yield values of 0.013 and 0.011 atomic units for  $\mathcal{K}$  in  $\text{PbZrO}_3$  and  $\text{CaTiO}_3$ , respectively. Moreover, the fact that these two systems possess similar values of their  $\mathcal{K}$  coefficient, while  $\text{CaTiO}_3$ , unlike  $\text{PbZrO}_3$ , does not adopt the complex  $Pbam$  phase as ground state, can also be understood thanks to additional information provided by these first-principles calculations, namely the computed energy first decreases, before increasing, with the magnitude of oxygen octahedral tiltings in  $\text{PbZrO}_3$  while such energy always increases with the strength of the oxygen octahedral tiltings in  $\text{CaTiO}_3$ . In other words, the “bare” octahedral tilting mode [i.e., the one related to  $E''_{\omega}(\lambda)$  in Sec. III E] is unstable with respect to the ideal cubic structure at the  $2\pi/a_{\text{lat}}$  (1/4, 1/4, 0)  $k$  point in  $\text{PbZrO}_3$  while it is stable in  $\text{CaTiO}_3$ .  $E''_{\omega}(\lambda)$  taken at  $\lambda = 1/2$  should thus be negative in  $\text{PbZrO}_3$  while being positive in  $\text{CaTiO}_3$ . To illustrate the consequence of such features, Fig. 6 displays the  $\kappa_{-}(\lambda)$  and  $\kappa_{+}(\lambda)$  eigenvalues of Eq. (12) when choosing  $H_{u\omega}$  being the same as in Fig. 4(b) as well as  $E''_u(\lambda)$  being identical to the one selected for case (1), but now taking a  $E''_{\omega}(\lambda)$  that has a *positive* value at  $\lambda = 1/2$  [while having the same value as in case (1) for the  $M$  point indexed by  $\lambda = 1$ ]. Figure 6 (which can be thought as corresponding to the case

of  $\text{CaTiO}_3$ ) reveals that the resulting  $\kappa_{-}$  at  $\lambda = 1/2$  is further away from the (minimum)  $\kappa_{-}$  at  $\lambda = 1$  than in Fig. 4(b) (which can be thought as representing the situation for  $\text{PbZrO}_3$ ). As a result and unlike in  $\text{PbZrO}_3$ , no realistic trilinear coupling between  $R_4^+$ ,  $\Sigma_2$ , and  $S_4$  can make  $Pbam$  become the ground state of  $\text{CaTiO}_3$ .

## V. CONCLUSIONS

In summary, we have introduced an elemental atomistic energy that exists in *all*  $ABO_3$  perovskites, which naturally explains, in a unified way, a variety of structurally complex phenomena. This energy couples, in a collaborative fashion, polar distortions driven by the  $A$ -site cations with  $O_6$ -rotational modes. Analytical derivations starting from this atomistic energy allow us to understand the nature and (in)stability of complex long-period phonons associated with  $k$ -points in the interior of the first Brillouin zone. Examples are the modes that play a key role in the stabilization of the antiferroelectric phases of  $\text{PbZrO}_3$ ,  $\text{PbHfO}_3$ ,  $\text{BiFeO}_3$ , and  $\text{BiFe}_{1/2}\text{Sc}_{1/2}\text{O}_3$ .

The newly-proposed couplings should be relevant to explain the behavior of perovskites in which the  $A$ -site cations have a tendency to move off-center (as it is, e.g., the case of those containing  $\text{Pb}^{2+}$  or  $\text{Bi}^{3+}$  cations) and also present oxygen-octahedral rotational instabilities. For instance, the proposed theory is most likely relevant to explain the unusual tilting pattern recently discovered in  $\text{Nd}_{1-x}\text{Li}_x\text{TiO}_3$  [30] as well as the large variety of antiferroelectric structures that are known to exist in  $\text{Pb}$ -based compounds (see, e.g., Ref. [14]). A structural determination of the  $A$ -site distortions and  $O_6$  tiltings would be required, at the experimental level, to confirm such a connection.

Finally, we demonstrated that our theory can also naturally explain the occurrence of incommensurate phases in perovskites. Indeed, we show that our work provides an unified description that brings together ferroelectric, antiferroelectric, antiferrodistortive ( $O_6$ -rotational), and incommensurate structures. Our results thus appear to be critical for deep understanding of the structural diversity in many perovskites, making a clear connection between the simplest and most exotic structures.

The structural instabilities driven by our proposed mechanism are *hybrid* in nature, in the sense that they combine (anti)polar and octahedra-rotational characters. Moreover, the coupling tends to favor long-period distortions corresponding to wave vectors that are away from the center or boundaries of the first Brillouin zone. In such cases, the pattern of  $O_6$  rotations is not perfect (we can say it is *truncated*) and the oxygen octahedra deform. Hence, our newly proposed coupling is most likely to be relevant in perovskites with relatively soft  $O_6$  groups. The existing examples suggest that this situation is favored by the presence of relatively large  $B$  cations in the perovskite structure.

Interestingly, it should also be possible to incorporate our interatomic couplings in atomistic approaches, such as the so-called effective Hamiltonians [27,38] [with, e.g., the  $\mathcal{K}$  coefficient of Eq. (1) being extracted from first-principles calculations], in order to, e.g., investigate properties of antiferroelectrics and incommensurate systems, as a function of temperature, applied electric fields, epitaxial strain, etc. Moreover, we have shown that it is straightforward to derive a continuum

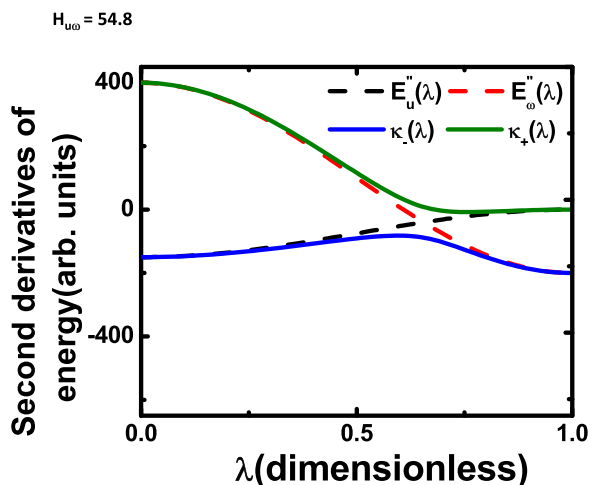


FIG. 6. Dependencies of  $E''_u(\lambda)$ ,  $E''_{\omega}(\lambda)$ ,  $\kappa_{-}(\lambda)$ , and  $\kappa_{+}(\lambda)$  along the  $\Sigma$  line for  $H_{u\omega} = 54.8$ , choosing here (in arbitrary units)  $E''_u(\lambda) = -192.5 - 2.5 \cos(\pi\lambda)$  and  $E''_{\omega}(\lambda) = +100 + 300 \cos(\pi\lambda)$ .  $\kappa_{-}(\lambda)$  and  $\kappa_{+}(\lambda)$  are given by Eq. (12).

(original) version of our coupling energy, as needed for the development of phenomenological Landau-Lifshitz theories.

### ACKNOWLEDGMENTS

We thank C. Cochard, G. Baldinozzi, M. Guennou, and D. Khalyavin for insightful discussions. This work is

supported by the Office of Basic Energy Sciences, under contract ER-46612 (K.P., B.X. and L.B.), the Luxembourg National Research Fund through the Pearl (J.I., Grant No. FNR/P12/4853155 CO-FERMAT) and Inter-Mobility (L.B. and J.I., Grant No. FNR/15/9890527 GREENOX) programs, and MINECO-Spain Grant MAT2013-40581-P (J.I.). Y.Y. and S.P. also acknowledge ONR Grant N00014-12-1-1034 and RFBR Grant 16-52-00072.

- 
- [1] X. Hao, *J. Adv. Dielectr.* **3**, 1330001 (2013).
- [2] B. Ma, D.-K. Kwon, M. Narayanan, and U. Balachandran, *J. Mater. Res.* **24**, 2993 (2009).
- [3] B. Ma, M. Narayanan, and U. Balachandran, *Mater. Lett.* **63**, 1353 (2009).
- [4] X. Hao, Y. Wang, L. Zhang, and S. An, *Appl. Phys. Lett.* **102**, 163903 (2013).
- [5] B. Peng, Q. Zhang, X. Li, T. Sun, H. Fan, S. Ke, M. Ye, Y. Wang, W. Lu, H. Niu, J. F. Scott, X. Zeng, and H. Huang, *Adv. Electron. Mater.* (2015).
- [6] J. Íñiguez, M. Stengel, S. Prosandeev, and L. Bellaiche, *Phys. Rev. B* **90**, 220103(R) (2014).
- [7] S. Prosandeev, C. Xu, R. Faye, W. Duan, H. Liu, B. Dkhil, P.-E. Janolin, J. Íñiguez, and L. Bellaiche, *Phys. Rev. B* **89**, 214111 (2014).
- [8] J. Hlinka, T. Ostapchuk, E. Buixaderas, C. Kadlec, P. Kuzel, I. Gregora, J. Kroupa, M. Savinov, A. Klic, J. Drahošoupil, I. Etxebarria, and J. Dec, *Phys. Rev. Lett.* **112**, 197601 (2014).
- [9] E. Cockayne and K. M. Rabe, *J. Phys. Chem. Solids* **61**, 305 (2000).
- [10] A. K. Tagantsev, K. Vaideeswaran, S. B. Vakhrushev, A. V. Filimonov, R. G. Burkovsky, A. Shaganov, D. Andronikova, A. I. Rudskoy, A. Q. R. Baron, H. Uchiyama, D. Chernyshov, A. Bosak, Z. Ujma, K. Roleder, A. Majchrowski, J.-H. Ko, and N. Setter, *Nat. Commun.* **4**, 2229 (2013).
- [11] J.-H. Ko, M. Gorny, A. Majchrowski, K. Roleder, and A. Bussmann-Holder, *Phys. Rev. B* **87**, 184110 (2013).
- [12] B. K. Mani, S. Lisenkov, and I. Ponomareva, *Phys. Rev. B* **91**, 134112 (2015).
- [13] K. M. Rabe, in *Functional Metal Oxides*, edited by S. B. Ogale, T. V. Venkatesan, and M. Blamire, Antiferroelectricity in Oxides: A Reexamination (Wiley 2013) and also available in <http://www.physics.rutgers.edu/karin>.
- [14] V. Yu, Topolov, E. S. Gagarina, and V. V. Demidova, *Ferroelectrics* **172**, 373 (1995).
- [15] S. A. Prosandeev, D. D. Khalyavin, I. P. Raevski, A. N. Salak, N. M. Olekhovich, A. V. Pushkarev, and Y. V. Radyush, *Phys. Rev. B* **90**, 054110 (2014).
- [16] D. D. Khalyavin, A. N. Salak, N. M. Olekhovich, A. V. Pushkarev, Yu. V. Radyush, P. Manuel, I. P. Raevski, M. L. Zheludkevich, and M. G. S. Ferreira, *Phys. Rev. B* **89**, 174414 (2014).
- [17] G. Baldinozzi, D. Grebille, Ph. Sciau, J.-M. Kiat, J. Moret, and J.-F. Bézar, *Acta Cryst. B* **56**, 570 (2000).
- [18] G. Baldinozzi, G. Calvarin, Ph. Sciau, D. Grebille, and E. Suard, *J. Phys.: Condens. Matter* **10**, 6461 (1998).
- [19] I. A. Kornev, L. Bellaiche, P.-E. Janolin, B. Dkhil, and E. Suard, *Phys. Rev. Lett.* **97**, 157601 (2006).
- [20] A. M. Glazer, *Acta Crystallogr. Sect. A* **31**, 756 (1975).
- [21] L. Bellaiche and J. Íñiguez, *Phys. Rev. B* **88**, 014104 (2013).
- [22] H. J. Zhao, J. Íñiguez, W. Ren, X. M. Chen, and L. Bellaiche, *Phys. Rev. B* **89**, 174101 (2014).
- [23] H. J. Zhao, W. Ren, Y. Yang, J. Íñiguez, X. M. Chen, and L. Bellaiche, *Nat. Commun.* **5**, 4021 (2014).
- [24] J. M. Rondinelli and C. J. Fennie, *Adv. Mater.* **24**, 1961 (2012).
- [25] Y. Yang, J. Íñiguez, A.-J. Mao, and L. Bellaiche, *Phys. Rev. Lett.* **112**, 057202 (2014).
- [26] D. Vanderbilt and W. Zhong, *Ferroelectrics* **206-207**, 181 (1998).
- [27] S. Prosandeev, D. Wang, W. Ren, J. Íñiguez, and L. Bellaiche, *Adv. Funct. Mater.* **23**, 234 (2013).
- [28] D. L. Corker, A. M. Glazer, W. Kaminsky, R. W. Whatmore, J. Dec, and K. Roleder, *Acta Cryst. B* **54**, 18 (1998).
- [29] P. Goudochnikov and A. J. Bell, *J. Phys.: Condens. Matter* **19**, 176201 (2007).
- [30] Y. Zhu, R. L. Withers, L. Bourgeois, C. Dwyer, and J. Etheridge, *Nat. Mat* **14**, 1142 (2015).
- [31] Strictly speaking, in these expressions we have to use, instead of the  $\omega$  pseudovector, the corresponding displacements of the oxygen ions associated with  $\omega$ , so that all the derivatives have the same units. Also, technically, one should include masses of ions in Eqs. (11), in order to be able to determine phonon frequencies. One can adopt the thinking here that these masses are, in fact, included in the  $F$ ,  $G$ , and  $H$  coefficients whenever we compare the  $\kappa_{-}$  eigenvalues with real phonon frequencies in the text—which will correspond to the second derivatives of Eqs. (11) being further divided by corresponding masses, in order to obtain the square of the phonon frequencies.
- [32] Ph. Ghosez, E. Cockayne, U. V. Waghmare, and K. M. Rabe, *Phys. Rev. B* **60**, 836 (1999).
- [33] Incommensurate solutions with  $0 < \lambda_{\min} < 1/2$  can be obtained for other choices of model parameters. Moreover, here we chose to focus on the  $\Sigma$  line, for simplicity, but it would be straightforward to extend our analysis to other lines joining the center and other boundary points of the Brillouin zone. This might permit an explanation of incommensurate phases reported in the literature, as those in Ref. [34].
- [34] G. Baldinozzi, Ph. Sciau, and A. Bulou, *J. Phys.: Condens. Matter* **9**, 10531 (1997).
- [35] V. Heine and J. D. C. McConnell, *J. Phys. C: Solid State Phys.* **17**, 1199 (1984).
- [36] L. D. Landau and E. M. Lifshitz, *Course of Theoretical Physics, Vol. 5, Statistical Physics* (Pergamon Press, Oxford, 1980), Part 1.
- [37] A. P. Levanuyk and D. G. Sannikov, *Fiz. Tverd. Tela* **18**, 423 (1976) [*Sov. Phys., Solid State* **18**, 245 (1976)].
- [38] W. Zhong, D. Vanderbilt, and K. M. Rabe, *Phys. Rev. B* **52**, 6301 (1995).